

# ScheduLeak: A Novel Scheduler Side-Channel Attack Against Real-Time Autonomous Control Systems

Chien-Ying Chen  
cchen140@illinois.edu  
University of Illinois at  
Urbana-Champaign

Sibin Mohan  
sibin@illinois.edu  
University of Illinois at  
Urbana-Champaign

Rakesh B. Bobba  
rakesh.bobba@oregonstate.edu  
Oregon State University

Rodolfo Pellizzoni  
rodolfo.pellizzoni@uwaterloo.ca  
University of Waterloo

Negar Kiyavash  
kiyavash@illinois.edu  
University of Illinois at  
Urbana-Champaign

## ABSTRACT

Real-time autonomous control systems are often the core of safety critical systems such as automotive systems, avionic systems, power plants and industrial control systems among others. While safety has traditionally been a focus in the design of these systems, security has often been an afterthought. In this paper we present a novel side-channel in real-time schedulers and algorithms that exploit it. In particular, we show that the scheduler side-channel can be used to obtain critical timing information that can aid other attacks. A complete implementation on both a simulator and real operating systems (*i.e.*, Real-Time Linux as well as FreeRTOS) is also presented to show the effectiveness of the algorithms. We use two attack scenarios on real hardware platforms to show the value of the extracted side-channel information (*i.e.*, aid attacks to reduce overheads and increase attack precision). The results indicate that our methods have a high success rate in reconstructing timing information and help advanced attacks in accomplishing their goals better.

## 1 INTRODUCTION

Autonomous control systems such as self-driving cars, medicine/vaccine delivery drones, space rovers (*e.g.*, NASA’s Opportunity and Spirit), industrial robots, autonomous tractors and military surveillance unmanned aerial vehicles (UAV), *etc.*, play a vital role in shaping today’s technological evolution from everyday living to space exploration. In such systems, tasks<sup>1</sup> delivering critical functionality rely on an operating system (typically a real-time operating system or an operating system that supports a real-time scheduling policy) to fulfill their timing requirements (*e.g.*, the task must complete within a predefined time limit). Oftentimes, these tasks (*e.g.*, system heartbeat keepers, PID control processes, sensor data collectors, motor actuators, *etc.*) are designed as real-time tasks and executed in a periodic fashion to guarantee responsiveness. However, as we point out in this paper, a scheduler side-channel exists in a preemptive, fixed-priority real-time task scheduler (the most common class of schedulers in real-time autonomous control systems). This scheduler side-channel can leak valuable timing behaviors of critical, high-priority real-time task(s) to unprivileged

low-priority tasks (that can be either a real-time task or a non-real-time task). We show that this side-channel can be exploited by a malicious/compromised low-priority task by simply observing its own execution intervals (*i.e.*, when the low-priority task itself is running and when it isn’t). In particular, we present novel attack algorithms, named “ScheduLeak”, that exploit the scheduler side-channel in real-time autonomous control systems. It is important to note that scheduler covert channels where two processes covertly communicate using the scheduler have long been known (*e.g.*, [8, 29, 33]). In contrast, our focus is on a side-channel that leaks execution timing behavior of critical, high-priority real-time tasks to any unprivileged, low-priority tasks.

Real-time tasks are usually constrained by their predefined periods, deadlines, the worst-case execution times (WCET) and real-time scheduling algorithms (*e.g.*, fixed-priority preemptive scheduling, earliest deadline first scheduling [17]). These real-time constraints help system designers analyze the system as a whole and ensure that all safety guarantees are met (*e.g.*, no real-time tasks will miss their deadlines). As a result, the system schedule (even a mix of both real-time and non-real-time tasks) becomes highly predictable. This predictability, though favorable for the system analysis and safety, is a double-edged sword. A smart attacker can exploit the scheduler side-channels and the predictable nature of the system schedule to recover execution behaviors of the targeted tasks (that we call “victim” tasks) *at runtime* (our attack algorithms achieve exactly that). Knowing the precise schedule of the victim real-time tasks enables the attacker to pinpoint the future execution patterns of such tasks. The adversary can then launch more devastating attacks at those future execution points of victim tasks.

For example, let us consider an unmanned aerial vehicle (UAV) executing a surveillance mission. The UAV runs a real-time operating system where multiple real-time tasks are used for navigation, communication and surveillance, *etc.* The UAV’s objective is to fly over some territory and capture high-resolution images when it reaches locations of interest. Assume that adversary has a user-space task in the system (for example, through a supply chain vulnerability). Here, the attacker’s goal is not to crash the UAV. Rather, the attacker wants to *stealthily* learn the locations of high-interest targets (where the surveillance camera is switched to a high-resolution image mode). This can be done by monitoring the memory usage behavior of the 30Hz real-time task that handles the images captured by the surveillance camera. In particular, a

<sup>1</sup>A task in typical real-time systems corresponds to a process/thread in generic operating systems. In this paper, we will use “task” and “process” interchangeably.

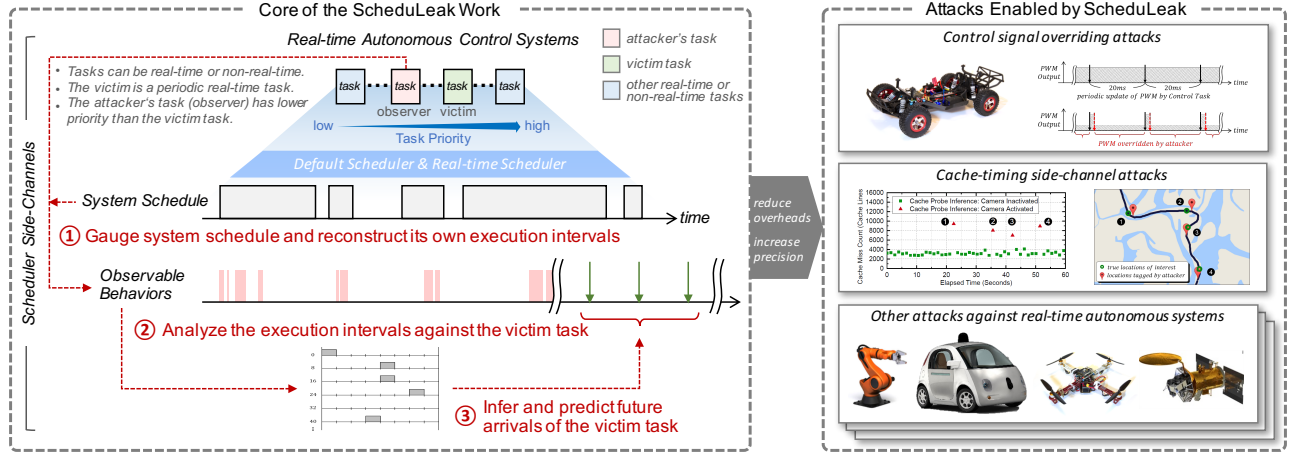


**Figure 1: Overview of this paper.** We focus on how an unprivileged, low-priority task can utilize the ScheduLeak algorithms to infer the execution behaviors of critical, high-priority real-time task(s). Two advanced attacks enabled by ScheduLeak are shown in this paper to demonstrate possible use cases of the extracted side-channel information.

cache-timing side-channel attack against such a victim task can be used to gauge its memory usage. A higher memory usage would indicate that a high-resolution image is being processed while a relatively lower memory usage shows that the operation of surveillance is inactive or on standby. However, as there are many tasks running in the same system, without knowing when the victim task is scheduled to run, a random sampling of the cache will result in noisy – often useless, data. By exploiting the extracted schedule information, the attacker can precisely execute prime and probe attacks [22, 23] before and after the victim task is executed. This attack is implemented and discussed in Section 5.2.

While most autonomous control systems with real-time tasks are vulnerable to the scheduler side-channel attacks presented in this paper, it is not trivial to learn and extract the exact times that the victim tasks are scheduled at *runtime*. This is because (i) the actual schedule depends on the system start-up and initialization and other environmental conditions and (ii) there may be multiple real-time and non-real-time tasks other than the victim task in the system that contribute to the uncertainty of the runtime schedule. In other words, even knowledge of all the predefined parameters (i.e., periods, deadlines and WCET) of all tasks alone is insufficient to reconstruct the actual schedule. While a privileged attacker might be able to extract the schedule directly from the scheduler, here we show that even an unprivileged attacker is able to learn the schedule of the victim task by using the proposed attack algorithms.

In this paper, we focus on autonomous control systems with a preemptive, fixed-priority real-time task scheduler [3, 17] since they are the most common class of real-time systems deployed in practice today [18]. Also, this class of systems (rather, the preemptive, fixed-priority scheduling algorithms) is most vulnerable to attacks since they are very *predictable* (by design). With the ScheduLeak algorithms, we are able to reconstruct the precise execution schedule of a periodic real-time victim task in the system by leveraging a compromised lower-priority user-space task. The ScheduLeak algorithms can carry out the attack while *staying within the execution time limits* of the compromised task. It is particularly crucial for the attacker to not perturb the strict timing properties of the

real-time autonomous control system, especially in the stage of reconstructing the information. Failing this will likely cause critical real-time functionality to fail or trigger a watchdog timeout that resets the system, leading to pre-mature detection of the attacker<sup>2</sup>. It has been reported that attackers had penetrated and stayed resident undetected in the system for *months* before they initiated the actual attack in the case of Stuxnet [6]. Once they had enough information about the precise nature of the system, they were able to craft effective attacks that were tailored to that particular system.

The ScheduLeak algorithms are implemented and evaluated on both a simulator and real hardware platforms running Real-Time Linux and FreeRTOS operating systems. Two attacks are demonstrated on the real hardware platforms to show that utilizing information gained from ScheduLeak can help stage other, more debilitating attacks in Section 5. Specifically we demonstrate how extracted schedule information can help (i) reduce attack overhead (in a control signal interleaving attack on a custom rover) and (ii) increase attack precision (in a cache-timing side-channel attack on a hardware-in-the-loop UAV platform). We also evaluate the performance and scalability of ScheduLeak in Section 6, along with a design space exploration. The evaluation results show that our methods are effective at reconstructing schedule information and provide valuable information for later attacks to better accomplish their attack goals. Note that, while two demonstrative attacks are shown in this paper, the use of the extracted schedule information is not limited to these cases.

Figure 1 shows an overview of the paper. The left side of the figure depicts the high-level concept of the proposed ScheduLeak attack and the right side illustrates possible attacks enabled by ScheduLeak. To summarize, the main contributions are:

- (1) Novel scheduler side-channel attack algorithms that can accurately reconstruct the execution timing behaviors of critical real-time tasks in real-time autonomous control systems (without privileged access). [Section 3]

<sup>2</sup>Most real-time autonomous control systems do not have an intrusion detection system (IDS). Yet, violating the real-time guarantees would be detected by the scheduler or any existing system error monitor.

- (2) Analyses and metrics to measure the accuracy in predicting the execution and timing properties of the victim tasks. [Section 4 and Section 6]

## 2 ADVERSARY AND SYSTEM MODEL

### 2.1 Adversary Model

In this paper, we are concerned with attacks that target a uniprocessor real-time autonomous control system<sup>3</sup>. The system consists of non-real-time and real-time (periodic or sporadic) tasks. We assume that an attacker is interested in targeting *one of the critical tasks in the system* that we henceforth refer to as a “*victim task*”. We also assume that the *victim task* is a *real-time, periodic* task. Many critical functions in real-time autonomous control systems are periodic in nature, say for sending control signals to actuate the system at a predetermined rate, *e.g.*, the code that controlled the frequency of the slave variable-frequency drives in the Stuxnet example [6]. Another example is engine control tasks in automotive systems. In all such cases, the period of the task is strictly related to the characteristics of the physical system; hence, we can assume that the attacker is able to gain knowledge of the victim task’s period from publicly available information (*e.g.*, [2]). However, the attacker does not know the initial conditions at system start-up<sup>4</sup>. All other tasks in the system can be either real-time or non-real-time, depending on the design of the system. Hence, the methods developed in this paper can target systems that have a mix of periodic, sporadic and non-real-time tasks.

The ultimate goal of the attacker varies with adversaries and the systems under attack. The attacker may plan to interfere with the operations of critical tasks (as mentioned earlier), or eavesdrop upon certain information via shared resources, or even carry out debilitating attacks at a critical juncture when the victim system is most vulnerable. Oftentimes, such attacks require the attacker to precisely gauge the timing properties of victim tasks - *i.e.*, when it is scheduled to run, how long it executes, *etc.* Hence, in this paper, the main goal of the attacker is to *precisely infer when the victim task is scheduled to run* in the near future.

Note that our focus in this paper is on how to reconstruct the timing behavior of a higher-priority, real-time victim task using the scheduler side-channel without violating the real-time constraints. We do this from the vantage point of a compromised, lower-priority (“observer”) task. We do not focus on *how* attackers get access to the observer task. They could use any number of known methods – from compromised insiders, to supply chain vulnerabilities in a multi-vendor development model (*e.g.*, as is usually practiced for large, complex systems such as aircraft, automobiles, industrial control systems, *etc.*) [24], to vulnerabilities in the software, network vulnerabilities, among others. Recent work has demonstrated that real-time autonomous control systems like commercial drones contain design flaws and hence are vulnerable to compromise [25, 28]. In particular, a system with a Linux kernel is arguably vulnerable

<sup>3</sup>Most real-time systems still use simple processors as part of their design. This is to ensure predictable behavior and due to the complexity of analyzing modern processors [20].

<sup>4</sup>Note that not all tasks have to start together at system startup; each periodic task is usually activated after some required initialization procedure, which can take a variable amount of time. Furthermore, a staggered startup of the tasks in the system significantly increases the challenge for would-be attackers in attempting to reconstruct the precise timing behavior of victim tasks. In this paper we show how to overcome such problems.

**Table 1: A Summary of the System Assumptions as well as an Attacker’s Capabilities and Goals.**

System Assumptions	
A1	All tasks are either non-real-time or real-time (periodic or sporadic) except the victim task which is a periodic real-time task.
A2	A preemptive, fixed-priority scheduler is used for all real-time tasks.
Attacker’s Capabilities (Requirements)	
R1	The attacker has the control of one user-space task (observer task) that has priority lower than the victim task.
R2	The attacker has knowledge of the victim task’s period.
R3	The attacker has access to a system timer on the system.
Attacker’s Goals	
G1	Being able to infer the victim task’s initial offset and predict future arrivals.

to attacks due to its complexity. The details of gaining access to an observer task are out of scope for this paper. Nevertheless, it is important to note that we do not require the observer task to be a privileged task in the system. A summary of assumptions, attacker’s capabilities and goals is given in Table 1.

### 2.2 Time Model

We assume that the attacker has access to a system timer on the target system and therefore time measured by the attacker has the resolution equal to or lower than this system timer. The timer can be either a software or a hardware timer (*e.g.*, a 64-bit *Global Timer* in FreeRTOS or a *CLOCK\_MONOTONIC*-based timer in Linux kernel). We consider a discrete time model [12]. We assume that a unit of time equals a timer tick of the timer the attacker has access to and the tick count (*i.e.*, time) is an integer. All system and task parameters are multiples of a time tick. We denote an interval starting from time point  $a$  and ending at time point  $b$  that has a length of  $b - a$  by  $[a, b)$  or  $[a, b - 1]$ .

### 2.3 Real-time Task Model

We consider a system consisting of real-time and non-real-time tasks in this paper. Along with a default scheduler for non-real-time tasks, a preemptive, fixed-priority scheduler (the most common class of real-time schedulers) is used to schedule the real-time tasks in the system. Here, we are only concerned with the real-time tasks since most modern system kernels handle the group of real-time tasks with a priority greater than the non-real-time tasks. As a result, non-real-time tasks do not influence the schedule of real-time tasks. Let’s consider the system containing  $n$  fixed-priority (*i.e.*, statically assigned) real-time tasks  $\Gamma = \{\tau_1, \dots, \tau_n\}$  [17]. A real-time task  $\tau_i$ ,  $1 \leq i \leq n$ , can be either a periodic or a sporadic task. A periodic task arrives regularly with a fixed length (*i.e.*, period) between adjacent arrivals. A sporadic task arrives at random time points with a given minimum length (*i.e.*, inter-arrival time) between adjacent arrivals. The victim task, denoted by  $\tau_v$ , is a periodic task, as stated in Section 2.1. Each real-time task is characterized by  $(p_i, d_i, e_i, a_i, pri_i)$  where  $p_i$  is the period (or the minimum inter-arrival time),  $d_i$  is the relative deadline<sup>5</sup>,  $e_i$  is the worst-case execution time (WCET)<sup>6</sup> [35],  $a_i$  is the initial task offset (*i.e.*, the arrival time) and  $pri_i$  is the priority. We assume that every

<sup>5</sup>The temporal constraint before which the task must complete execution – missing these deadlines can result in failures in real-time autonomous control systems.

<sup>6</sup>In real-time systems the practice is to reason about *guaranteed* WCET for predictability. The system must always allocate computation resources for WCET.

real-time task has a distinct period<sup>7</sup> and that a task's deadline is equal to its period<sup>8</sup> [17]. We use the same symbol  $\tau_i$  to represent a task's job (or instance) for simplicity of notation.

We further assume that each task is assigned the priority  $pri_i$  using an assignment algorithm (e.g., rate-monotonic [17], criticality-based, table-based), and that task priorities are distinct. Let  $hp(\tau_i)$  denote the set of tasks that have higher priorities than that of  $\tau_i$  and  $lp(\tau_i)$  denote the set of tasks that have lower priorities than  $\tau_i$ .

We define an "execution interval" of a task  $\tau_i$  to be an interval of time  $[a, b]$  during which the task runs continuously. For example, if  $\tau_i$  runs to its worst case execution time  $e_i$ , then for a particular instance of  $\tau_i$ , the length of the execution interval equals  $e_i$  if  $\tau_i$  is not preempted during the execution. If  $\tau_i$  is preempted then the execution will be partitioned into multiple execution intervals, each of which has length less than  $e_i$ .

## 2.4 Observer Task

As previously mentioned, we refer to the lower-priority task that the attacker controls as an "observer task" and it is denoted by  $\tau_o \in \Gamma$ . The only constraint we place on  $\tau_o$  is that it has a lower priority than the victim task,  $pri_o > pri_v$ . The observer task can be either a real-time or a non-real-time task. Recall that non-real-time tasks have lower priority than real-time tasks, so it is preferable for the attacker to compromise and utilize a non-real-time observer task. In contrast, being a periodic real-time task is a more restrictive condition since it reduces the flexibility available to an attacker (this will be clearer as we introduce the algorithms). That is, the case where a periodic observer task with a period  $p_o$  and priority  $pri_o$  can succeed, a non-real-time or a real-time sporadic (given the same  $p_o$  as the minimum inter-arrival time and the same priority  $pri_o$ ) observer task can also succeed. Therefore, when analyzing the attack capability in Section 4, we will consider a real-time periodic observer task (or a real-time sporadic observer task running at a constant inter-arrival time). Both cases (i.e., the observer task being a real-time task and a non-real-time task) are covered in the demonstrations on real hardware platforms presented in Section 5.

In this paper, we use the observer task to infer the initial offset  $a_v$  that can be used to predict future arrivals of the victim task. We let the observer task "monitor" its own execution intervals by using a system timer. The main concept here is that the intervals when the observer task is active (i.e., no higher-priority task is running) cannot contain the victim task's execution or its arrival time point since the victim would have preempted the observer task. However, there are also other higher-priority tasks that can impact the observer task's execution behaviors. To the attacker, the challenge is to then filter out unnecessary information (about other higher-priority tasks) and extract the correct information about the victim task. This is explained in the following section.

<sup>7</sup>It is common practice in the design of real-time tasks to ensure that tasks have distinct periods/priorities. For example, AUTOSAR (a standardized automotive software architecture) tools map runnables/functions activated by the same period to a single task to reduce context switch/preemption overheads.

<sup>8</sup>This is a common assumption in most preemptive, fixed-priority real-time systems – intuitively, it just means that at any point in time, there is only one instance of a real-time task that is active/waiting to execute.

## 3 SCHEDULEAK

### 3.1 Overview

We now introduce the core algorithms of the ScheduLeak attacks. As mentioned earlier, the goals of the attacker are: (a) collect execution intervals that contain the victim task's schedule information and (b) analyze the intervals to infer the initial offset for the victim. Since all tasks do not start together at system start-up, knowledge of the initial offset is required along with period information to infer the future time execution instants. A high-level overview of the various analyses stages is introduced next (also depicted in Figure 1).

First, the observer task measures and reconstructs its own execution intervals (i.e., when it itself is active). We then introduce the notion of a "schedule ladder diagram" – a timeline that is divided into windows that match the repeating period of the victim task, and map the measured intervals onto this timeline. A "union" of the various periods on the timeline allows us to extract the initial offset for the victim task. This information is then used to predict the future arrivals of the victim. Since the victim task is also periodic in nature, the offset from the start of the section of the timeline that it falls under directly translates to the offset from startup when the first instance of the victim task executed. Hence, the steps in our proposed ScheduLeak attack algorithms are:

- (1) Reconstruct execution intervals of the observer task: the observer task utilizes a system timer to reconstruct its execution intervals. [Section 3.2]
- (2) Analyze the execution intervals: the execution intervals are organized in a schedule ladder diagram for further analysis of the victim task's arrivals and initial offset. [Section 3.3]
- (3) Infer the victim task's initial offset: in the final step, the attacker infers the initial offset of the victim task by extracting the information from the schedule ladder diagram. The future arrivals of the victim task are predicted by using the inferred initial offset. [Section 3.4]

### 3.2 Reconstruction of Execution Intervals

The first step is to reconstruct the observer task's execution intervals (i.e., the intervals when the observer task is itself active). We

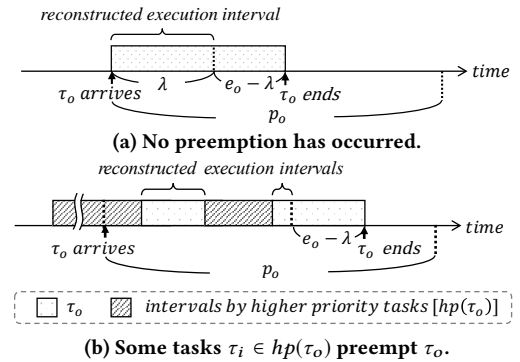


**Figure 2: Examples of reconstructed execution intervals of the periodic real-time observer task,  $\tau_o$ , in a period when it is (a) executing and (b) preempted. One execution interval is reconstructed for every invocation of the Algorithm 1. The total length of the reconstructed execution intervals is  $\lambda$  that leaves  $e_o - \lambda$  for  $\tau_o$  to perform original task functions.**

achieve this by implementing a function in the observer task that keeps track of time read from the system timer. For instance, when the observer task executes, it keeps polling the system timer. When it gets preempted, the polling obviously stops. When it is scheduled to run again (indicating that the higher-priority tasks, potentially including the victim task, have completed execution) the polling starts again. Hence, the continuous active execution intervals of the observer task can be reconstructed by examining the polled time stamps. The function is shown in Algorithm 1 in Appendix A.

Algorithm 1 returns one execution interval of the observer task for every invocation. If required, the attacker can invoke this algorithm multiple times to reconstruct the execution intervals in detail. However, if a real-time observer task is used, then this might take up significant amount of execution time in a period – perhaps more than what was budgeted for the observer task. To satisfy the real-time constraints (*i.e.*, all real-time tasks must meet their deadlines), the real-time observer task should not run more than its worst-case execution time,  $e_o$ . Furthermore, even if the attacker does not exceed the allocated execution budget for itself, it may want to save some budget for other purposes such as performing the analyses to reconstruct the timing information of the victim. Hence, we define a parameter,  $\lambda$ , whose value is set by the attacker, to limit the running time of the aforementioned algorithm for the real-time periodic observer task. This “maximum reconstruction time”,  $\lambda$ , is an integer in the range  $0 \leq \lambda \leq e_o$ . Hence, the total length of the reconstructed execution intervals is  $\lambda$  in each execution period and this leaves the timespan  $e_o - \lambda$  for the observer task to carry out other computations. As a result, the service levels guaranteed by the original (clean) system is still maintained – thus reducing the risk of triggering system errors. On the flip side, the algorithm may not be able to capture all possible execution intervals and this could reduce the fidelity/precision of the final results. Section 4.2 discusses how to compute good values for  $\lambda$ . Figure 2 shows examples of reconstructed execution intervals.

### 3.3 Analysis of Execution Intervals

Once the observer task’s execution intervals are reconstructed, we analyze the data to extract the information about the victim task. We do this by organizing the obtained execution intervals into a timeline split into lengths of the victim task’s period  $p_v$  (recall that  $p_v$  is one of the known quantities for the attacker). The purpose of this step is to place the execution intervals of the observer task within the periodic windows of the victim task. The timeline with length of the victim task’s period allows the attacker to see how the observer task’s execution intervals are influenced by the victim task as well as other higher-priority tasks.

To better illustrate the idea of the timeline and the proposed algorithms, we will use a “schedule ladder diagram” (defined below) to represent the construction of the timeline in this paper. The rows in the schedule ladder diagram can, of course, be merged into a single-line timeline (and is just an analytical “trick”). A schedule ladder diagram is a skeleton consisting of a set of adjacent timelines of equal lengths – that match the victim task’s period  $p_v$ . The start time of the top section can be an arbitrary point in time assigned by the attacker (*e.g.*, the time instant when the algorithms are first invoked). The columns in the schedule ladder diagram are “unit

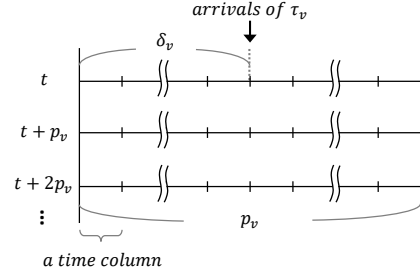


**Figure 3: The skeleton of a schedule ladder diagram. It is used by the observer to organize its execution intervals. The start time  $t$  of the schedule ladder diagram (*i.e.*, the beginning of the top timeline) is an arbitrary point in time, as assigned by the attacker. The width of each timeline matches the victim task’s period  $p_v$ . The relative offset between the start time  $t$  and the true arrival column is defined by  $\delta_v$ .**

time columns”. So, there are  $p_v$  time columns. The skeleton of a schedule ladder diagram is illustrated in Figure 3. From the diagram, plotted based on  $p_v$ , we make the following observation:

**OBSERVATION 1.** Any schedule ladder diagram of a task  $\tau_v$  must contain exactly one arrival/execution instance of  $\tau_v$  in every row. All arrivals of  $\tau_v$  are located in the same time column.

This observation is true because  $\tau_v$  is a periodic task that arrives every  $p_v$  time units and the schedule ladder diagram is plotted with its interval equal to  $p_v$ . We define the column where the arrivals of the victim task are located as the “true arrival column”, denoted by  $\delta_v$ . Thus, the correlation between the initial offset  $a_v$  and the true arrival column  $\delta_v$  can be derived by  $(t + \delta_v - a_v) \bmod p_v = 0$ , where  $t$  represents the (arbitrary) start time of the schedule ladder diagram assigned by the attacker. This is also depicted in Figure 3.

The observation also means that the time columns  $[\delta_v, \delta_v + bcet_v)$ , where  $bcet_v$  is the best case execution time of  $\tau_v$  (*i.e.*, the shortest possible execution time of  $\tau_v$ ), will always be occupied by either the victim task or other higher-priority task executions. From this observation, we define the following theorem for placing the observer task’s execution intervals on this schedule ladder diagram.

**THEOREM 3.1.** The interval (time columns)  $[\delta_v, \delta_v + bcet_v)$  does not contain any execution interval of the observer task.

The proof of Theorem 3.1 is given in Appendix B.1. Note that  $\delta_v$  and  $bcet_v$  are unknown to the attacker. If we place the obtained execution intervals of the observer task on the schedule ladder diagram and calculate the union of those execution intervals for every time column, then, based on Theorem 3.1, there must exist an empty interval of continuous time columns of which the length is equal to or greater than  $bcet_v$ . Here, an empty interval represents the time columns where the observer task is always inactive and hence do not contain any execution intervals of the observer task. Those empty time columns are candidates for containing the true arrival time of the victim task. There may also exist time columns that are empty due to other higher-priority tasks. Yet, since other tasks have distinct arrival periods (or random arrivals for real-time sporadic tasks and non-real-time tasks), those empty time columns tend to be scattered, compared to  $[\delta_v, \delta_v + bcet_v)$ , and are expected to be eliminated as more execution intervals of the

observer task are collected. In practice, our results indicate that this process works effectively and is mostly stabilized after an attack duration of  $5 \cdot LCM(p_o, p_v)$ . To this end, it's easier to think of the problem as the process of eliminating those time columns that are not true arrival columns for the victim. We use the following theorem to remove these “false” time columns.

**THEOREM 3.2.** *The time columns in which there exists at least one execution interval of the observer task cannot be true arrival columns.*

The proof of Theorem 3.2 is presented in Appendix B.2. Based on Theorem 3.2, we can remove corresponding time columns when an execution interval of the observer is placed on the schedule ladder diagram. Ultimately, the attacker can eliminate most of the false time columns, thus leaving only a small portion of the time columns (containing  $[\delta_v, \delta_v + bcet_v)$  based on Theorem 3.1) to infer the victim task's initial offset. The algorithm to infer the victim task's initial offset is introduced next.

### 3.4 Inference of Initial Offset and Future Arrival Instants

We now get to the final step – inferring the future arrival instants of the victim task – our original objective. But, first, we need to calculate the initial offset of the victim task. What we get from the schedule ladder diagram (*i.e.*, the timeline of periods of the victim task) is a set of “empty” intervals of candidate time columns that contains the true arrival column of the victim. The number of empty intervals depends on the number of collected execution intervals as well as the “noise” introduced by other, higher-priority, tasks (hence, there is no guarantee that all false empty intervals can be eliminated in the end). Since the false empty intervals tend to be scattered, compared to  $[\delta_v, \delta_v + bcet_v)$ , due to distinct arrival periods for other real-time periodic tasks or random arrivals for real-time sporadic tasks, we take the largest empty interval as our inference for the interval that may contain the true arrival column of the victim task. While this strategy is not always guaranteed to succeed, our evaluation (Sections 5 and 6) shows that we are able to reconstruct the future arrival instants for victim tasks with a high degree of precision. We then pick the start of this empty interval as the inferred true arrival column, denoted by  $\hat{\delta}_v$ . The inferred initial offset, denoted by  $\hat{a}_v$ , can then be derived as  $\hat{a}_v = (t + \hat{\delta}_v) \bmod p_v$ , where  $t$  represents the start time of the schedule ladder diagram.

Now, the future arrivals of the victim task can easily be computed by  $t + \hat{a}_v + p_v \cdot T$ ,  $T \in \mathbb{N}$ , where  $t$  is the starting time of the schedule ladder diagram,  $\hat{a}_v$  is the inferred initial offset of  $\tau_v$ ,  $p_v$  is the period of  $\tau_v$  and  $T$  is the desired arrival number. The result of this calculation is the *exact time of the  $T^{th}$  arrival of the victim task*.

Note that we are able to draw all of these inferences by just using observations from the *observer task only* and no other knowledge of runtime behavior of any other task! To further help understand the aforementioned steps of the ScheduLeak algorithms, an example is given in Appendix C.

## 4 ANALYSIS OF ALGORITHMS

### 4.1 Analyzing Attack Capability

We now discuss how to determine the attack capability of the observer task against the victim task. That is, in this context, whether

the observer task's observation contains the arrival information of the victim task. This analysis is mainly for the observer task being a periodic real-time task since its observability is restricted by the real-time constraints. A non-real-time observer task is not limited by a period and the attack capability depends on its runtime duration (this will be explained later in this section). Therefore, understanding the correlation of the schedule between the observer task and the victim task is vital.

From Observation 1, we know that the periodic arrivals of  $\tau_v$  land at exactly the same time column in the schedule ladder diagram. Thus, a conservative condition ensuring that the scheduled, anticipated execution intervals of the observer task can overlap the victim task's arrival column is when those scheduled execution intervals appear in all possible time columns in the schedule ladder diagram. Furthermore, when considering both  $\tau_v$  and  $\tau_o$  as periodic tasks, they have a hyper-period (*i.e.*, the length when the schedule of the given tasks repeats) computed by their *least common multiple*,  $LCM(p_o, p_v)$ . Therefore, we have the following observation about the relationship between  $\tau_o$  and  $\tau_v$  on the schedule ladder diagram.

**OBSERVATION 2.** *In the schedule ladder diagram, the offset between the time column of each observer task's arrival (*i.e.*, the scheduled execution) and the true arrival column repeats after  $LCM(p_o, p_v)$ .*

This observation also means that the coverage of the time columns by the observer repeats every  $LCM(p_o, p_v)$ . Thus, for the observer task to observe all  $p_v$  time columns, we have the following theorem:

**THEOREM 4.1.** *If the given observer task  $\tau_o$  and the victim task  $\tau_v$  satisfy the inequality* 
$$e_o \geq GCD(p_o, p_v) \quad (1)$$
 *then the scheduled execution of  $\tau_o$  is guaranteed to appear in all time columns of the schedule ladder diagram of  $\tau_v$ .*

The proof of Theorem 4.1 is given in Appendix B.3. From Theorem 4.1, we can find that the observer task's execution is able to observe some time columns more than once when  $e_o > GCD(p_o, p_v)$ . If  $e_o \geq 2 \cdot GCD(p_o, p_v)$ , the observer task observes all time columns more than once. The redundant coverage means that the true arrival column will be observed more frequently comparing to lower ratio of  $e_o$  to  $GCD(p_o, p_v)$ .

To better profile the observer task's coverage, we further define the *coverage ratio* that depicts the observer task's capability against the victim task as follows

**Definition 4.2.** (Coverage Ratio) The *coverage ratio*, denoted by  $\mathbb{C}(\tau_o, \tau_v)$ , is computed by 
$$\mathbb{C}(\tau_o, \tau_v) = \frac{e_o}{GCD(p_o, p_v)} \quad (2)$$

The *coverage ratio* can be loosely interpreted as the proportion of the time columns that are observable by the observer task in the *schedule ladder diagram*. If all  $p_v$  time columns are observed by the observer task's observation, then  $\mathbb{C}(\tau_o, \tau_v) \geq 1$ . Otherwise  $0 \leq \mathbb{C}(\tau_o, \tau_v) < 1$ . Note that  $\mathbb{C}(\tau_o, \tau_v)$  can be greater than one if  $e_o$  is greater than  $GCD(p_o, p_v)$ . It means that the observer task can observe all time columns more than once with greater  $e_o$ . It's worth mentioning that  $p_o$  can be ignored in the case of a non-real-time observer task. Then the coverage ratio becomes  $\frac{e_o}{p_v}$ , where  $e_o$  can be interpreted as the non-real-time observer task's runtime duration that depends on how long the attacker resides in the

system. Therefore, we have the following theorem to determine the observer task's capability against the victim task:

**THEOREM 4.3.** *Given the observer task  $\tau_o$  and the victim task  $\tau_v$ , the capability of  $\tau_o$  against  $\tau_v$  is determined by:*

- (1) *If  $\mathbb{C}(\tau_o, \tau_v) \geq 1$   
then the execution of  $\tau_o$  captures true arrival time column of  $\tau_v$ .*
- (2) *If  $\mathbb{C}(\tau_o, \tau_v) < 1$   
then the execution of  $\tau_o$  may or may not capture true arrival time column of  $\tau_v$ .*

The proof of Theorem 4.3 is shown in Appendix B.4. Note that the second condition in Theorem 4.3 does not necessarily mean that  $\tau_v$  is absolutely not inferable by  $\tau_o$ . It only implies that  $\tau_o$ 's execution cannot appear in all possible time columns. Depending on the degree of the *coverage*, the attacker may still be able to observe the true arrival column.

## 4.2 Choosing Maximum Reconstruction Duration $\lambda$

Recall that, the maximum reconstruction duration  $\lambda$  is used to limit the amount of execution time in a period taken by a periodic real-time observer task for running the attack algorithms. The remaining execution time  $e_o - \lambda$  can be used by the attacker to deliver the original functionality of  $\tau_o$  while making progress on the capturing of execution data. As the attacker wants to stay stealthy and minimize disruption to the original functionality during this phase, it is desirable to use smaller  $\lambda$  (i.e., larger  $e_o - \lambda$ ) values. Here, we discuss how to choose the value of  $\lambda$  for a given periodic real-time observer task  $\tau_o$  and a victim task  $\tau_v$ .

In Section 4.1, we defined the notion of *coverage ratio* that profiles the observer task's attack capability. It can be interpreted as the number of times that the execution of the observer task can observe all  $p_v$  time columns in the schedule ladder diagram. Since a one-time coverage of all  $p_v$  time columns is sufficient to hit the true arrival column, the additional coverage is redundant and can be traded for other purposes. Based on this idea, we use the following theorem to determine the value for  $\lambda$ .

**THEOREM 4.4.** *Given the observer task  $\tau_o$  and the victim task  $\tau_v$ , the minimum value of  $\lambda$  for the best possible coverage is determined by:*

$$\lambda = \begin{cases} \text{GCD}(p_o, p_v) & \text{if } \mathbb{C}(\tau_o, \tau_v) \geq 1 \\ e_o & \text{otherwise} \end{cases} \quad (3)$$

The proof is given in Appendix B.5.

## 4.3 Observer Task: Real-time vs. Non-real-time

The ScheduLeak algorithms can be applied to an observer task being either a real-time task or a non-real-time task since the computation only relies on the victim task's period. Yet, given the same target system, the latter (non-real-time) performs better than the former as the real-time observer task is restricted by its real-time constraints. This inference can also be drawn from the coverage ratio we discussed in Section 4.1. The non-real-time observer task potentially has no limits on its coverage ratio as well as the maximum reconstruction duration  $\lambda$  and is only limited by how long the attacker stays in the system. In contrast, special care needs to

be taken by the attacker when a periodic real-time observer task is engaged. As a result, the introduced algorithms and theorems cover the worst case condition when carrying out the reconnaissance.

## 5 EVALUATION WITH CASE STUDIES

The ScheduLeak algorithms are implemented on two operating systems with a real-time scheduling capability: (i) Real-Time Linux (i.e., Linux with the PREEMPT\_RT patch) [30] and (ii) FreeRTOS [7]. We first aim to demonstrate the feasibility of such algorithms on realistic platforms in this section. In what follows, two attack cases are presented. They benefit from the information obtained by the proposed algorithms since they learn critical time points in the schedule and better utilize such information to accomplish their primary attack goals. The demo videos for the attacks can be found at <https://scheduleak.github.io/>.

**Note:** The main/novel contribution of this paper is the discovery of the scheduler side-channels in real-time autonomous control systems and the development of the ScheduLeak algorithms described thus far. The attacks in Sections 5.1 and 5.2 are just *examples* that show *how to use the extracted side-channel information* to improve the fidelity/success of other attacks and is not intended to demonstrate complete end-to-end attacks against such systems.

### 5.1 Reducing Attack Overheads

Let's consider a real-time autonomous subsystem that controls some actuators. The attacker wants to be able to override the control – for the purpose of creating an illusion of bad control by causing (temporary or permanent) misbehavior or even taking over the control of the system for a short time span. A brute force strategy of excessively overriding the control signals will not work in this scenario because its high attack overhead can cause some real-time tasks to miss their deadlines and lead to system failures. Therefore, utilizing information from reconnaissance attacks like ScheduLeak to help reduce attack overhead is particularly crucial when attacking a system containing real-time tasks.

Specifically, let's consider a remotely controlled rover or a quadcopter. This type of systems is typically equipped with one or more electronic speed controllers (ESCs) and servos that receive pulse-width modulation (PWM) signals from the control board to drive its motors or actuators (e.g., wheels, propellers, steering). A periodic real-time task is usually used to update the PWM value in the hardware. For example, the rover system we use in this demonstration has a periodic real-time task running at 50Hz (period is 20ms). Its job is to periodically update the PWM output as displayed in Figure 4(a). Since this actuator refresh rate (i.e., 50Hz or 400Hz) is commonly used in a control system, the attacker can easily infer the period of such tasks from publicly available information.

Figure 4(b) and (c) show that the PWM output may be overridden by overwriting it with a different value to the PWM hardware block. However, without exact schedule information, the attacker can either send the updates at random instants (Figure 4(b)) or periodically but at an arbitrary offset that leads to ineffective attacks. On the other hand, Figure 4(c) displays that the attacker can carefully issue an PWM update *right after the original update* to override the PWM output. By doing so, an attacker can potentially take over



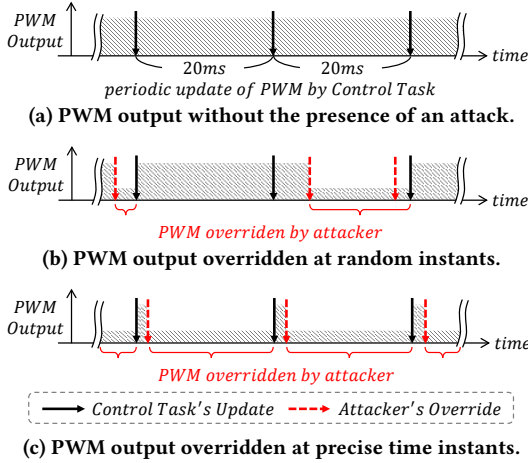


**Figure 4: An illustration of a PWM channel output on a rover system. The PWM output is updated periodically by a 50Hz task. (b) shows that an naive attack issuing the PWM updates at random instants may not be effective. (c) shows that the PWM output can be overridden by carefully issuing the PWM update right after the original update.**

control of the actuators. Yet, precise *future timing* knowledge of such a task is required to accomplish this goal.

**5.1.1 Setup.** We implement this attack on a real remote rover and a quadcopter. To illustrate, we will focus on the case of the rover here. Its control system is built with a Raspberry Pi 3 Model B board [26]. A Navio2 module board [21] that encapsulates various inertial sensors is attached to the Raspberry Pi board to enable the control capability. The board is configured to use only a single core to match the assumed system model. The system runs Real-Time Linux (*i.e.*, Raspbian, kernel 4.9.45 with PREEMPT\_RT patch) with an APM flight stack [2] that is one of the most popular open-source code stack in the remote control community. It consists of a set of real-time tasks to perform control-related jobs such as refreshing GPS coordinates, decoding remote control commands, performing PID calculation and updating output signals. As mentioned earlier, we are targeting the task that periodically updates the PWM output (*i.e.*, the victim task with  $p_v = 20ms$ ). The victim task handles two PWM output channels for steering and throttle. In this attack, we intend to override both PWM output channels.

We assume that the attacker has got into the system, as we explained in Section 2.1. Here, we restrict the observer’s capability to a non-real-time process in Linux. As a result, the observer task has the priority lower than all the real-time tasks in the system. In this implementation, the observer task uses a system call, `clock_gettime()`, to obtain clock counts from `CLOCK_MONOTONIC` to measure and reconstruct its own execution intervals.

**5.1.2 Attack Manifestation and Results.** The attack begins after the rover starts moving. We let the observer task run the ScheduLeak algorithms for 1 second and it successfully infers the victim task’s arrival time with a precision of 99.85% (defined formally in Section 6.1). Utilizing this precise schedule information, the attacker submits the forged PWM output only after the inferred time instants as shown in Figure 4(c). By probing the PWM signals, we

observe that the overridden PWM signals are active 85% of the time. As a result, we see that the rover no longer responds to the remote controller. Instead, the rover is driven by the attacker’s commands. To further reduce the attacker’s footprint, the attacker’s task remains idle between two PWM updates, which leads to a CPU utilization of 2.6%. As a comparison, a brute-force approach takes up 77.9% CPU utilization (*i.e.*, all available CPU resource) to achieve the same effect.

## 5.2 Increasing Attack Precision

Here, we present the attack introduced in Section 1. A UAV executing a surveillance mission is considered. It captures high resolution images when flying over locations of interest. In this case, the attacker’s goal is to stealthily learn the locations targeted by the UAV. The strategy is to monitor when the surveillance camera on the UAV is switched to a execution mode in which high-resolution images are being processed. This can be done by exploiting a cache-timing side-channel attack to gauge the coarse-grained memory usage behavior of the task that handles the images (victim). A high cache usage by the victim task would indicate that a high-resolution image is being processed, otherwise it would use less cache memory. However, a random sampling of the cache will result in noisy (and often useless) data since there exist other tasks in the system. In contrast, knowing when the task is scheduled to run allows the attacker to execute prime and probe attacks [22, 23] very close to the victim task’s execution. As a result, a scheduler side-channel attack like the one presented in this paper that learns the schedule timing information is needed. In what follows, both, the results with and without information from ScheduLeak, are demonstrated.

**5.2.1 Setup.** We use a Zedboard running the FreeRTOS OS to simulate the control system on a UAV. The demonstration is done using hardware-in-the-loop (HIL) simulation where the system is attached to a computer for the flight route and to display its trajectory. The system consists of an image processing task handling photos at a rate of 30Hz (*i.e.*, the victim task,  $p_v = 33ms$ , which is known to the attacker) and four other real-time tasks (unknown to the attacker) – all running in a periodic fashion. The victim task reacts differently based on a preloaded list of GPS coordinates that are of interest to the victim. It processes a large size of data when the UAV reaches a coordinate on the list. Other real-time tasks consume differing amounts of memory. We assume that the attacker enters the system as one of the low-priority periodic tasks (*i.e.*, the observer task,  $p_o = 40ms$ ) by exploiting some existing vulnerabilities. Here, the observer task is used to run both the ScheduLeak attack and the cache-timing side-channel attack. The observer task uses a 64-bit Global Timer (GT) that is shared in FreeRTOS on Zedboard to measure and reconstruct its own execution intervals. We further assume that the attacker is able to obtain GPS coordinates via other means. Ultimately, the attacker’s goal is to combine the inference of the victim task’s behavior and the obtained GPS coordinates to identify the locations of high-interest along the flight path.

**5.2.2 Attack Results.** First, let’s consider an attacker who does not have access to ScheduLeak-ed information. The attacker launches the cache-timing side-channel attack at arbitrary instants due to a lack of precise timing information. As shown in Figure 5(a), this



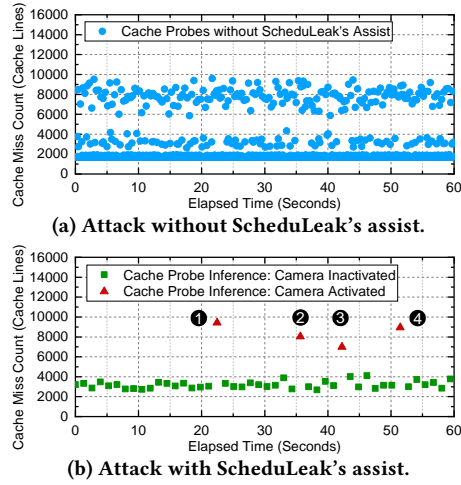


Figure 5: Results of the cache-timing side-channel attacks in Section 5.2. (a) demonstrates that a random mechanism launching the attack at arbitrary instants will lead to many indistinguishable cache usage results. (b) shows a successful attack in which four camera activation events (numbered by 1 to 4) are identified from the cache probes using precise time information inferred by ScheduLeak.

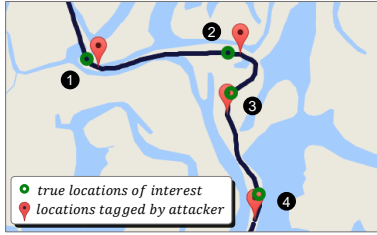


Figure 6: Data recorded by the HIL simulator for the attack in Figure 5(b). The bold line is the UAV's trajectory, the green circles represent the true locations-of-interest to the UAV, and the red pins (numbered by 1 to 4) are the high-interest locations inferred by the attacker. The result shows that the attacker's inference matches the ground truth.

produces many cache probes (it is hard to distinguish the cache usage of the victim task from other tasks in Figure 5(a)) and results in an unsuccessful attack.

Then, we launch an attack after running ScheduLeak attack in advance. The ScheduLeak attack algorithms run at the beginning to learn the victim task's future invocations. In this case, the algorithms yield a precision of 99.998% for the inference of the victim task (see Section 6.1 for the definition). Once the analysis is complete, the attacker moves to the next stage to monitor the victim task's memory usage behavior. With the precise schedule information, the attacker is able to launch the cache-timing side-channel attack right before and after the victim is executed and skip those instants that are irrelevant. Figure 5(b) shows the result of the precise cache probe against the victim task. We see that the attack greatly reduces the noise caused by other real-time tasks and is able to precisely identify the victim task's memory usage behavior. The attacker can therefore determine that the camera is activated if the

victim task's memory usage is high or deactivated if the memory usage is low. As a result, four camera activation instants can be identified from the spikes shown in Figure 5(b). Combining this with the real-time GPS data, the locations of high-interest can be uncovered. Figure 6 shows the UAV's trajectory, actual locations of interest (red markers) and the attacker's estimated points of interest (green dots). The results suggest that the attack is successful and the ScheduLeak attack can increase the effectiveness of the cache-timing side-channel attack in achieving its goal.

## 6 PERFORMANCE EVALUATION

### 6.1 Evaluation Metrics

To evaluate ScheduLeak, we define the following two metrics:

(i) **Inference Success Rate:** We define an inference to be successful if attacker is able to *exactly* infer the victim task's initial offset (recall from Section 3.4 that once we know the initial offset, we can easily predict the future arrival instants). Therefore, the result of an inference is either true or false. The inference success rate is an *average of the true/false results* for a given test condition from a set of task sets.

(ii) **Inference Precision Ratio:** In the case that the inference is not exact, we define a metric to evaluate the degree of the inference precision (*i.e.*, how close we got to the actual values). In this paper, the inference target is the initial offset of the victim task. We first compute the distance between the inference and the true value by  $\epsilon = |\hat{a}_v - a_v|$ , where  $a_v$  is the initial offset of the victim task and  $\hat{a}_v$  is the inferred initial offset (calculated by our analyses). We then define the inference precision ratio:

*Definition 6.1.* (Inference Precision Ratio) The inference precision ratio, denoted by  $\mathbb{I}_v^o$ , is computed by

$$\mathbb{I}_v^o = \begin{cases} 1 - \frac{p_v - \epsilon}{\frac{p_v}{2}} & \text{if } \epsilon > \frac{p_v}{2} \\ 1 - \frac{\epsilon}{\frac{p_v}{2}} & \text{otherwise} \end{cases} \quad (4)$$

$p_v$  is the period of the victim task. Thus, the inference precision ratio is a real number within  $0 \leq \mathbb{I}_v^o \leq 1$ . It allows us to know how close the inference is to the true initial offset.  $\mathbb{I}_v^o = 1$  indicates that the inference of the initial offset  $a_v$  is absolutely correct.

### 6.2 Evaluation Setup

We use simulations of real-time tasks to evaluate our algorithms. The time resolution in the simulations is  $0.1ms$ . We only include real-time tasks (both periodic and sporadic) in the simulations since they are the real load in the system that impacts the real-time task schedule. Also, a periodic real-time observer task is considered here because it represents the worst case attack scenario for the adversary, as we discussed in Section 4.3. We test our algorithms with randomly generated synthetic task sets. (**Note:** this is a standard method for evaluating algorithmic facets of real-time systems. Using synthetic task sets gives us the ability to also explore a wide variety of situations.) We use the commonly used rate-monotonic algorithm [17] to assign the priorities of real-time tasks, *i.e.*, a task with a shorter period is assigned a higher priority. We only pick those task sets that are schedulable<sup>9</sup> by preemptive, fixed-priority

<sup>9</sup>During the design of real-time systems, engineers test what is known as the "schedulability" of the system – essentially, whether given the current set of tasks and the

scheduling algorithms. The task sets are grouped by CPU utilization from  $[0.001 + 0.1 \cdot x, 0.1 + 0.1 \cdot x]$  where  $0 \leq x \leq 9$ . For example, the  $[0.501, 0.6]$  group contains the task sets that occupy 50.1% to 60% of CPU utilization<sup>10</sup>. Each utilization group consists of 6 subgroups that have a fixed number of tasks from 5, 7, 9, 11, 13 and 15 respectively. Each subgroup contains 100 task sets. In each task set, 50% of the tasks are generated as periodic tasks (i.e., 3, 4, 5, 6, 7 and 8 periodic tasks for each subgroup respectively) while the rest of the tasks are generated as sporadic tasks. The initial arrival time (i.e., task offset) for a task is randomly selected between 0 and the task's period (i.e.,  $0 \leq a_i < p_i$ ). In the case of sporadic tasks, we take the generated task period as the minimum inter-arrival time.

The observer task and the victim task are assigned when generating the task sets. Since only the tasks that have higher priorities influence the observations, we skip the generation of lower-priority tasks  $lp(\tau_o)$ . As a result, the observer task always has the lowest priority (i.e.,  $pri_o = 1$ ) in these generated task sets. For the victim task, two conditions are considered: (i)  $pri_v = 2$  and (ii)  $pri_v = |hp(\tau_o)|$ . It is to test the two boundary conditions (i.e., when no task and the most tasks exist in between the observer task and the victim task). Further, we set the coverage ratio to be  $\mathbb{C}(\tau_o, \tau_v) \geq 1$  when generating the task sets, except for evaluating the impact of the coverage ratio. This is because we want to evaluate whether the algorithms can truly produce confident inferences while the attacker has the theoretical guarantee of the attack capability (i.e., having full coverage of all  $p_v$  time columns, as per Theorems 4.1 and 4.3). The maximum construction duration  $\lambda$  is set based on Theorem 4.4. Therefore,  $\lambda = GCD(p_o, p_v)$ .

For varying the execution times of the tasks and adding jitter to the inter-arrival times (for the sporadic tasks), we use the normal and Poisson distributions respectively. Note that Poisson distribution is used for inter-arrival time variation because the probability of each occurrence (i.e., each arrival of the sporadic task) is independent in such a distribution model. First, a schedulable task set is generated (using the aforementioned parameters). Then, for a task  $\tau_i$ , the average execution time is computed by  $wcet_i \cdot 80\%$ , where 80% is chosen empirically. Next, we fit a normal distribution  $\mathcal{N}(\mu, \sigma^2)$  for the task  $\tau_i$ . We let the mean value  $\mu$  be  $wcet_i \cdot 80\%$  and find the standard deviation  $\sigma$  with which the cumulative probability  $P(X \leq wcet_i)$  is 99.99%. As a result, such a normal distribution produces variation such that 95% of the execution times are within  $\pm 10\% \cdot wcet_i$ . To ensure that the task set remains schedulable, we adjust the maximum modified execution time to be equal to WCET if it exceeds WCET. For sporadic tasks, the average inter-arrival time is computed by  $p_i \cdot 120\%$ , where 120% is chosen empirically. We use a Poisson distribution of  $\lambda = p_i \cdot 120\%$  to generate the varied inter-arrival times during the simulation. Similarly, so as to not violate the given minimum inter-arrival time for a sporadic task, we regenerate the modified inter-arrival time if it drops below  $p_i$ .

system setup (processor, etc.), will all instances of all real-time tasks complete before their respective deadlines. If even a single instance of a single real-time task does not meet its deadline then the system is deemed unschedulable and *unsafe*. There exists a large body of work in the real-time system domain aimed at verifying the schedulability of real-time systems [3, 18].

<sup>10</sup> Grouping the task sets by utilization is a standard practice in real-time system domain – in practice, it allows us to evaluate the efficacy of our solutions based on the load on the system – a higher utilization represents a heavily loaded system and vice versa.

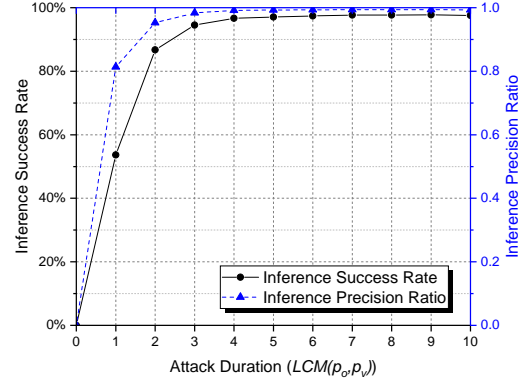


**Figure 7: The results of the success rate and the inference precision ratio by running the algorithms for different lengths of time. It indicates that longer attack durations can increase the chance of success and yield better inference precision. The points are connected only as a guide.**

### 6.3 Experiment Results

**6.3.1 Attack Duration.** Our first goal is to understand the effects of the duration of attacks. Recall that the coverage of the schedule ladder diagram repeats every  $LCM(p_o, p_v)$  (Observation 2). In the best case (i.e., no task preempts the observer task except the victim task),  $LCM(p_o, p_v)$  is the minimum duration needed to observe all  $p_v$  time columns and get the right inference. Therefore, we use  $LCM(p_o, p_v)$  as the unit of time spent on the attack to evaluate the algorithms. In this experiment, we generate task sets as explained in Section 6.2 and run the ScheduLeak algorithms with a fixed duration of  $10 \cdot LCM(p_o, p_v)$ . Figure 7 and Table 2 (Appendix D) show the results of this experiment.

In Figure 7, each point of the inference precision ratio is the mean of the individual inference precision ratio of 12000 task sets for a given attack duration. The results suggest that the longer the attack id sustained, the higher success rate and precision ratio the algorithms can achieve. It is because a longer attack time means more execution intervals are reconstructed by the observer task.

On the other hand both success rate and precision ratio plateau after  $5 \cdot LCM(p_o, p_v)$  with the success rate and the precision ratio higher than 97% and 0.99 respectively. This shows that the proposed algorithms can produce inference with precision in a very short time and the additional gains obtained from running longer are minuscule. For this reason, we will evaluate the algorithms with a duration of  $10 \cdot LCM(p_o, p_v)$  in the rest of the experiments below.

**6.3.2 The Number of Tasks and Task Set Utilization.** Next, we evaluate the impact of (a) the number of tasks in a task set and (b) the task set utilization. Figure 8 displays a 3D wire frame graph that shows the averaged inference precision ratio for each combination of the number of tasks and the task utilization subgroup. The results suggest that (i) the inference precision ratio decreases as the number of tasks in a task set increases and (ii) the inference precision ratio increases as the task set utilization increases. The worst inference precision ratio happens when there are 15 tasks in a task set with the utilization group  $[0.001, 0.1]$ , – these are boundary conditions for both the number tasks and the utilization in this experiment. The

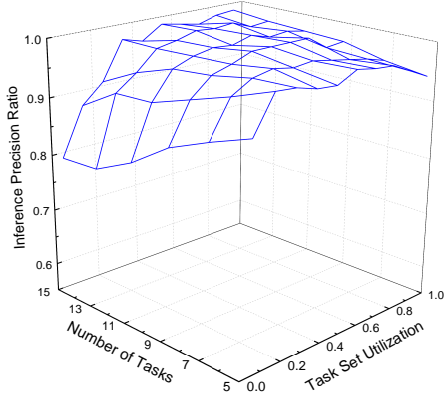


**Figure 8: The impact of the number of tasks in a task set and the task set utilization. The left X-axis is the number of tasks in a task set, the right X-axis is the task set utilization and Y-axis is the inference precision ratio. The result shows that the algorithms perform better with small number of tasks and high task set utilization.**

impact of the number of tasks is straightforward as having more tasks in  $hp(\tau_o)$  means that the observer task will be preempted more frequently. This makes it hard for the observer task to eliminate the time columns that are not true arrival columns; thus the inference precision ratio is reduced. For the impact of the task set utilization, having low utilization implies that the execution times of the tasks are small and there exists a lot of gaps in the schedule. Hence, the observer may get many small and scattered empty-intervals. Since we let the algorithms pick the largest interval to infer the true arrival column, multiple small intervals are problematic – the algorithm has a hard time picking the right interval that contains the true arrival. Hence the errors are compounded.

**6.3.3 Priority of the Victim Task.** From the previous experiments we learned that the number of tasks has an impact on the inference performance. However, the relative position of the victim task should also be taken into account when the number of tasks varies. Therefore, we focus on the victim task’s position (*i.e.*, its priority in a task set) here to further analyze what influences the algorithms. As stated in Section 6.2, we consider two boundary conditions for the victim task’s position: (i)  $pri_v = 2$  and (ii)  $pri_v = |hp(\tau_o)|$ . Figure 9 and Figure 10 present the experiment results for the two conditions. Figure 9 shows that the huge drop in Figure 8 as the number of tasks increases is mainly caused by the condition  $pri_v = |hp(\tau_o)|$  when the victim task has the highest priority. Figure 10 also gives the similar indication that the drop in low utilization groups in Figure 8 is a result of the condition  $pri_v = |hp(\tau_o)|$ . It’s worth noting that, since we use the rate-monotonic algorithm to assign the priority,  $pri_v = 2$  means that the victim task has a large period, hence potentially has greater execution time. It is good for the algorithms as we pick the largest interval to make an inference in the last step. In contrast,  $pri_v = |hp(\tau_o)|$  means that the victim task has the smallest period in a task set. This would cause problems when trying to pick the right interval for the inference.

**6.3.4 Task Sets with Sporadic, Periodic and Mix of Both.** Here, we examine the impact of the mix of sporadic tasks and periodic tasks.

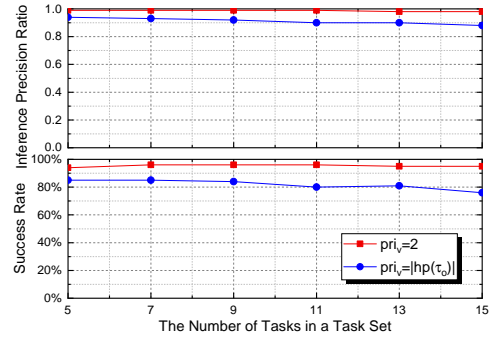


**Figure 9: The impact of the victim task’s position in the task sets grouped by the number of tasks in a task set. The results suggest that a victim task with higher priority makes it hard for the algorithms to make a correct inference. This result stands throughout different number of tasks in a task set.**

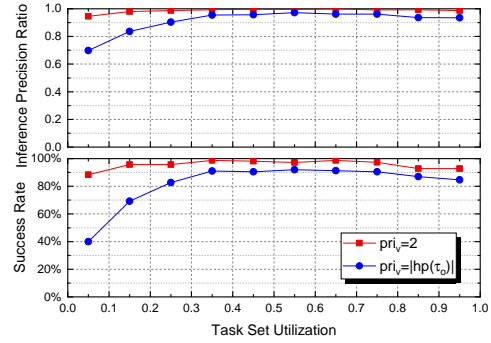


**Figure 10: The impact of the victim task’s position in the task sets grouped by the task set utilization. It shows that a high priority victim task with low task set utilization reduces the inference performance. This explains the huge drop that occurs in Figure 8.**

We generate task sets with 0%, 25%, 50%, 75% and 100% sporadic tasks in a task set. The rest of the tasks in a task set are periodic tasks. The group of 0% indicates that all tasks are periodic tasks and the group of 100% means that all tasks are sporadic tasks in a task set. The results are shown in Figure 11. Comparing the result of all periodic tasks (the 0% group) and the result of all sporadic tasks (the 100% group), we can find that the *algorithms perform better with more sporadic tasks*. It shows an ascending trend as the proportion of sporadic tasks increases. However, the change in the performance is less than 1%, which is subtle. Hence, our inference algorithms are fairly agnostic to the actual mix of sporadic/periodic tasks in the system.

**6.3.5 Coverage Ratio and The Maximum Reconstruction Duration.** The experiments above show that the algorithms can reach certain inference success rate and precision when  $\mathbb{C}(\tau_o, \tau_v) \geq 1$  and  $\lambda = \text{GCD}(p_o, p_v)$ . However, attackers may face a victim system where  $\mathbb{C}(\tau_o, \tau_v) < 1$ . That is, the observer task’s execution is not guaranteed to appear in all  $p_v$  time columns (*i.e.*, condition 2 in Theorem 4.3). To evaluate the performance of the algorithms against such a case, we generate task sets with  $0 < \mathbb{C}(\tau_o, \tau_v) < 1$  (thus

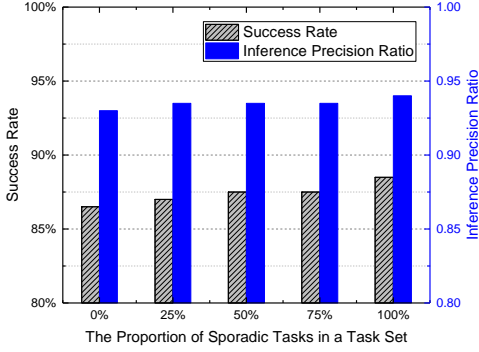


**Figure 11: The impact of sporadic tasks and periodic tasks. It indicates that the algorithms perform better with sporadic tasks, with a (slightly) ascending trend as the proportion of sporadic tasks increases.**

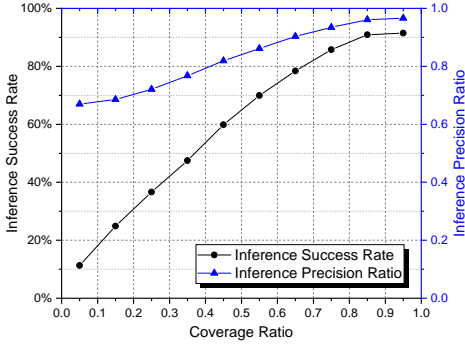


**Figure 12: The performance of the algorithms when the coverage ratio is less than one (condition 2 in Theorem 4.3).**

$\lambda = e_o$ ) and run the algorithms for a duration of  $10 \cdot \text{LCM}(p_o, p_v)$ . In this experiment, task sets are grouped by coverage ratio from  $[0.001 + 0.1 \cdot x, 0.1 + 0.1 \cdot x]$  where  $0 \leq x \leq 9$ . Figure 12 shows the results. It suggests that the attacker may fail to infer the victim task's initial offset when the coverage ratio is low. When the observer has about half coverage of the time columns (the group of  $[0.401, 0.5]$ ), it yields 59.9% in success rate and 0.819 for the averaged inference precision ratio. As more time columns are observed by the observer task, the precision and success rate increase. This is because higher coverage ratios give the algorithms a higher chance to capture the true arrival column and remove others. As a result, the inference success rate is about proportional to the coverage ratio.

## 7 DISCUSSION AND RELATED WORK

The problem of information leakage via side-channels has been well studied in the literature. For instance, it has been shown that cache-based side-channels can be invaluable for information leakage [10, 15, 22, 23]. With the advent of multi-tenant public clouds, cache-based side-channels and their defenses have received renewed interest (e.g., [11, 27, 34, 41]). Other types of side-channels such as differential power analysis (e.g., [13]), electromagnetic and frequency analysis (e.g., [1, 31]) have also been studied. Our focus here is on scheduler side-channels in real-time autonomous control systems.

There has also been some work on information flow via schedulers. Kadloor *et al.* [14] presented a methodology for quantifying side-channel leakage for first-come-first-serve and time-division-multiple-access schedulers. Gong and Kiyavash [9] carried out analysis for deterministic work-conserving schedulers and discovered a lower bound for the total information leakage. The problem where two users form a covert channel in a shared scheduler to steal private information from a secure system is studied by Ghassami *et al.* [8]. There are also other work focusing on real-time schedulers. Son *et al.* [29] highlighted the susceptibility of the fixed-priority schedulers (with the rate-monotonic algorithm) to covert timing-channel attacks. Völz *et al.* [33] examined covert channels between different priorities of real-time tasks and proposed a solution to avoid such covert channels by modifying fixed-priority scheduling and altering thread blocks that potentially leak information with the idle thread. Other work by Völz *et al.* [32], the authors studied information leakage over shared-resource covert channels and proposed a transformation of resource locking protocols to preserve the confidentiality guarantees of the schedulers. While the previous works focused on covert channels in some schedulers, our focus is on novel side-channels in real-time schedulers where an unprivileged low-priority task can infer the execution timing behaviors of high-priority real-time task(s). Also, in contrast to covert channels which rely on actively preempting real-time tasks, the scheduler side-channel in our work does not violate any real-time constraint and the observer task only knows when itself is active.

Our preliminary, unpublished work [4, 5] explored the possibility of reconstructing the complete task schedule of a real-time system. However, that goal is accomplished under a different, stronger attacker model that requires (i) the system to contain all periodic real-time tasks, (ii) the attacker to know the profile of the entire task set before attacking the system and (iii) the observer task to be the *lowest* priority task in the system. In contrast, in this paper we focus on the much harder problem (targeting a more realistic system model) and explore what an attacker is capable of inferring with minimum knowledge and resources in the system.

The integration of security into real-time schedulers is a developing area of research. Mohan *et al.* [20] offered a consideration of real-time system security requirements as a set of scheduling constraints. They introduced a modified fixed-priority scheduling algorithm that integrates security levels into scheduling decisions. Pellizzoni *et al.* [24] extended the above scheme to a more general task model and also proposed an optimal priority assignment method that determines the task preemptibility. Some researchers also have focused on defense techniques for real-time systems (e.g., [16, 19, 36, 38–40]). However, these solutions do not protect the systems from the ScheduLeak attack. The most closely related solution is by Yoon *et al.* [37]. They proposed a randomization protocol for a preemptive, fixed-priority scheduler (with the rate-monotonic algorithm) to obfuscate the repeated schedule patterns. Nevertheless, their algorithms are only feasible on systems that are made up of all periodic tasks while our work targets a mixed system (*i.e.*, all periodic real-time, sporadic real-time and non-real-time tasks are allowed). This leaves most real-time autonomous control systems still vulnerable to the introduced ScheduLeak attack.



## 8 CONCLUSION

Successful security breaches in autonomous control systems (including cyber-physical systems) with real-time properties can have catastrophic effects. In many such systems, knowledge of the precise timing information of critical tasks could be beneficial to adversaries. Our work in this paper demonstrates how to capture this schedule timing information in a *stealthy* manner – i.e., without being detected or causing any perturbations to the original system. Designers of such systems now need to be cognizant of such attack vectors and design the system to include countermeasures that can thwart potential intruders. The end result is that safety-critical systems with real-time requirements can be more robust to security threats overall.

## REFERENCES

- [1] Dakshi Agrawal, Bruce Archambeault, Josyula R. Rao, and Pankaj Rohatgi. 2003. The EM Side-Channel(s). In *the 4th International Workshop on Cryptographic Hardware and Embedded Systems*.
- [2] ArduPilot Autopilot Suite. 2018. <http://ardupilot.org/>. (2018).
- [3] Giorgio C. Buttazzo. 1997. *Hard Real-Time Computing Systems: Predictable Scheduling Algorithms and Applications*.
- [4] Chien-Ying Chen, Amiremad Ghassami, Sibin Mohan, Negar Kiyavash, Rakesh B. Bobba, and Rodolfo Pellizzoni. 2016. ScheduLeak: An Algorithm for Reconstructing Task Schedules in Fixed-Priority Hard Real-Time Systems. (2016).
- [5] Chien-Ying Chen, Amiremad Ghassami, Stefan Nagy, Man-Ki Yoon, Sibin Mohan, Negar Kiyavash, Rakesh B Bobba, and Rodolfo Pellizzoni. 2015. Schedule-based side-channel attack in fixed-priority real-time systems. (2015).
- [6] Nicolas Falliere, Liam Murchu, and Eric Chien (Symantec). 2011. W32.Stuxnet Dossier. [http://www.symantec.com/content/en/us/enterprise/media/security\\_response/whitepapers/w32\\_stuxnet\\_dossier.pdf](http://www.symantec.com/content/en/us/enterprise/media/security_response/whitepapers/w32_stuxnet_dossier.pdf). (2011).
- [7] FreeRTOS. 2018. <http://www.freertos.org/>. (2018).
- [8] AmirEmad Ghassami, Xun Gong, and Negar Kiyavash. Capacity limit of queueing timing channel in shared FCFS schedulers. In *2015 IEEE International Symposium on Information Theory (ISIT)*.
- [9] Xun Gong and Negar Kiyavash. 2014. Timing Side Channels in Shared Queues. *CoRR* abs/1403.1276 (2014). <http://arxiv.org/abs/1403.1276>
- [10] Wei-Ming Hu. 1992. Lattice scheduling and covert channels. In *Research in Security and Privacy, Proceedings., IEEE*.
- [11] G. Irazoqui, M. S. Inci, T. Eisenbarth, and B. Sunar. 2014. Fine Grain Cross-VM Attacks on Xen and VMware. In *Big Data and Cloud Computing (BdCloud), IEEE*.
- [12] Damir Isovic. 2001. *Handling sporadic tasks in real-time systems: combined offline and online approach*. Mälardalen University.
- [13] Ke Jiang, L. Batina, P. Eles, and Zebao Peng. 2014. Robustness Analysis of Real-Time Scheduling Against Differential Power Analysis Attacks. In *2014 IEEE Computer Society Annual Symposium on VLSI (ISVLSI)*, 450–455. <https://doi.org/10.1109/ISVLSI.2014.11>
- [14] Sachin Kadloor, Negar Kiyavash, and Parv Venkatasubramanian. 2013. Mitigating Timing Side Channel in Shared Schedulers. *CoRR* abs/1302.6123 (2013). <http://arxiv.org/abs/1302.6123>
- [15] John Kelsey, Bruce Schneier, David Wagner, and Chris Hall. 1998. Side channel cryptanalysis of product ciphers. In *European Symposium on Research in Computer Security*.
- [16] M. Lin, L. Xu, L. T. Yang, X. Qin, N. Zheng, Z. Wu, and M. Qiu. 2009. Static Security Optimization for Real-Time Systems. *IEEE Transactions on Industrial Informatics* 5, 1 (Feb 2009), 22–37. <https://doi.org/10.1109/TII.2009.2014055>
- [17] C. L. Liu and J. W. Layland. 1973. Scheduling algorithms for multiprogramming in a hard real-time environment. *J. ACM* (1973).
- [18] Jane W. S. Liu. 2000. *Real-Time Systems*. Prentice Hall.
- [19] Sibin Mohan, Stanley Bak, Emiliano Betti, Heechul Yun, Lui Sha, and Marco Caccamo. 2013. S3A: Secure System Simplex Architecture for Enhanced Security and Robustness of Cyber-Physical Systems. In *ACM Conference on High Confidence Networked Systems*.
- [20] Sibin Mohan, Man-Ki Yoon, Rodolfo Pellizzoni, and Rakesh Bobba. 2014. Real-Time Systems Security through Scheduler Constraints. In *Euromicro Conference on Real-Time Systems*. <https://doi.org/10.1109/ECRTS.2014.28>
- [21] Navio2 Module Board. 2018. <https://emlid.com/navio/>. (2018).
- [22] Dag Arne Osvik, Adi Shamir, and Eran Tromer. 2006. Cache attacks and countermeasures: the case of AES. In *Cryptographers' Track at the RSA Conference*. Springer, 1–20.
- [23] Dan Page. 2002. Theoretical use of cache memory as a cryptanalytic side-channel. *IACR Cryptology ePrint Archive* 2002 (2002), 169.
- [24] Rodolfo Pellizzoni, Neda Paryab, Man-Ki Yoon, Stanley Bak, Sibin Mohan, and Rakesh Bobba. 2015. A Generalized Model for Preventing Information Leakage in Hard Real-Time Systems. In *IEEE Real-Time Embedded Technology and Applications Symposium*.
- [25] Johann-Sebastian Pleban, Ricardo Band, and Reiner Creutzburg. 2014. Hacking and securing the AR. Drone 2.0 quadcopter: investigations for improving the security of a toy. In *IS&T/SPIE Electronic Imaging*. International Society for Optics and Photonics, 90300L–90300L.
- [26] Raspberry Pi. 2018. <https://www.raspberrypi.org/>. (2018).
- [27] Thomas Ristenpart, Eran Tromer, Hovav Shacham, and Stefan Savage. 2009. Hey, you, get off of my cloud: exploring information leakage in third-party compute clouds. In *Proceedings of the 16th ACM conference on Computer and communications security*. ACM.
- [28] Fred Samland, Jana Fruth, Mario Hildebrandt, Tobias Hoppe, and Jana Dittmann. 2012. AR. Drone: security threat analysis and exemplary attack to track persons. In *Proceedings of the SPIE*, Vol. 8301.
- [29] Joon Son and J. Alves-Foss. 2006. Covert Timing Channel Analysis of Rate Monotonic Real-Time Scheduling Algorithm in MLS Systems. In *IEEE Information Assurance Workshop*. <https://doi.org/10.1109/IAW.2006.1652117>
- [30] The Real Time Linux Collaborative Project. 2018. <https://wiki.linuxfoundation.org/realtime/>. (2018).
- [31] Chin Chi Tiu. 2005. *A New Frequency-Based Side Channel Attack for Embedded Systems*. Technical Report.
- [32] Marcus Völz, Benjamin Engel, Claude-Joachim Hamann, and Hermann Härtig. 2013. On Confidentiality Preserving Real-Time Locking Protocols. In *IEEE, RTAS*.
- [33] Marcus Völz, Claude-Joachim Hamann, and Hermann Härtig. 2008. Avoiding timing channels in fixed-priority schedulers. In *ACM Symposium on Information, Computer and Communication Security*.
- [34] Zhenghong Wang and Ruby B. Lee. 2007. New cache designs for thwarting software cache-based side channel attacks. In *Proc. of the 34th annual ACM international symposium on Computer architecture*.
- [35] Reinhard Wilhelm, Jakob Engblom, Andreas Ermedahl, Niklas Holsti, Stephan Thesing, David Whalley, Guillem Bernat, Christian Ferdinand, Reinhold Heckmann, Tulika Mitra, Frank Mueller, Isabelle Puaut, Peter Puschner, Jan Staschulat, and Per Stenström. 2008. The Worst-case Execution-time Problem - Overview of Methods and Survey of Tools. *ACM Trans. Embed. Comput. Syst.* 7, 3, Article 36 (May 2008), 36:1–36:53 pages.
- [36] Tao Xie and Xiao Qin. 2007. Improving Security for Periodic Tasks in Embedded Systems Through Scheduling. *ACM Trans. Embed. Comput. Syst.* (2007).
- [37] M. K. Yoon, S. Mohan, C. Y. Chen, and L. Sha. 2016. TaskShuffler: A Schedule Randomization Protocol for Obfuscation against Timing Inference Attacks in Real-Time Systems. In *IEEE Real-Time and Embedded Technology and Applications Symposium*.
- [38] Man-Ki Yoon, Sibin Mohan, Jaesik Choi, Jung-Eun Kim, and Lui Sha. 2013. SecureCore: A Multicore-based Intrusion Detection Architecture for Real-Time Embedded Systems. In *IEEE Real-Time Embedded Technology and Applications Symposium*.
- [39] Man-Ki Yoon, Sibin Mohan, Jaesik Choi, and Lui Sha. 2015. Memory Heat Map: Anomaly Detection in Real-Time Embedded Systems Using Memory Behavior. In *Proc. of the ACM Design Automation Conference*.
- [40] Mohammad Mehdi Zeinali Zadeh, Mahmoud Salem, Neeraj Kumar, Greta Cutulenco, and Sebastian Fischmeister. 2014. SIPTA: Signal Processing for Trace-based Anomaly Detection. In *Proc. of the International Conference on Embedded Software*.
- [41] Yinqian Zhang, Ari Juels, Michael K. Reiter, and Thomas Ristenpart. Cross-VM Side Channels and Their Use to Extract Private Keys. In *Proceedings of the 2012 ACM Conference on Computer and Communications Security*.

## A ALGORITHM FOR RECONSTRUCTING AN EXECUTION INTERVAL

**Algorithm 1** Reconstructing An Execution Interval  $\mathbb{E}(e_o, e'_o, \lambda)$

---

```

{GT : global timer (system timer)}
{e_o : the worst case execution time of  $\tau_o$ }
{e'_o : remaining execution time of present job of  $\tau_o$ }
{\lambda : maximum reconstruction duration in a period}
{t_stop : stop time when  $\lambda$  is met}
{t_0, t_{-1} : present and last time stamps}
{t_begin, t_end : start, end time of the detected interval}
1: t_0 = GT
2: t_begin = t_0
3: t_stop = t_begin + e'_o - (e_o - \lambda)
4: duration = 0
5: while duration ≤ loop execution time unit and t_0 < t_stop do
6:   t_{-1} = t_0
7:   t_0 = GT
8:   duration = t_0 - t_{-1}
9: end while
10: if duration > loop execution time unit then
11:   t_end = t_{-1}
12: else
13:   t_end = t_0
14: end if
15: e'_o = e'_o - (t_end - t_begin)
16: return {t_begin, t_end, e'_o}

```

---

Algorithm 1 takes the observer task's worst case execution time  $e_o$ , the remaining execution time of the present instance  $e'_o$  and the maximum reconstruction duration  $\lambda$  as inputs. It outputs the start time  $t_{begin}$  and end time  $t_{end}$  of the detected execution interval as well as the updated remaining execution time of the present instance  $e'_o$ . Lines 1–4 initialize the variables to be used by the algorithm. Specifically, line 3 computes the point in time (the stop condition) when the algorithm reaches the given maximum reconstruction duration  $\lambda$  for the present instance. Lines 5–9 are used to detect a preemption and check if current time exceeds the computed stop time point. These lines keep track of the time difference between each loop by reading present time from a global timer (i.e., a system timer) and comparing it to the time from the previous loop. If the time difference exceeds what we anticipate (the execution time of the loop), we know that a preemption occurred (i.e., one or more higher-priority tasks executed). The loop exits either when a preemption is detected or the present time exceeds the computed stop time point. Lines 10–12 determine the end time of the reconstructing execution interval. If the loop exits because of a preemption, the last time point before the preemption is taken as the end time of that execution interval (line 11). Otherwise, no preemption is detected, all  $\lambda$  duration is used up and the latest time point is taken as the end time of the execution interval (line 13). Line 15 updates the remaining execution time of the present job for the next invocation. Line 16 returns the reconstructed execution interval (its start time  $t_{start}$  and end time  $t_{end}$ ) and the updated remaining execution time.

## B PROOFS FOR THEOREMS

### B.1 Proof for Theorem 3.1

From Observation 1, the victim task  $\tau_v$  arrives regularly at time column  $a_v$ . Upon an arrival of  $\tau_v$ , it is scheduled to be executed at the arrival column/instant  $\delta_v$ . If there exists lower priority tasks  $lp(\tau_v)$  in execution at  $\delta_v$  column, the victim task preempts such tasks until it finishes its job with length of  $bect_v$  at a minimum. In the case that there exists higher priority tasks  $hp(\tau_v)$  that are executing or arriving during  $[\delta_v, \delta_v + bect_v)$ , the victim task  $\tau_v$  is preempted. Under this circumstance, if the observer task  $\tau_o$  had arrived during  $[\delta_v, \delta_v + bect_v)$ , as a lower priority task, it is also preempted. Therefore, the time columns  $[\delta_v, \delta_v + bect_v)$  cannot contain the execution intervals of the observer task.

### B.2 Proof for Theorem 3.2

From Theorem 3.1, the observer task is always preempted within time columns  $[\delta_v, \delta_v + bect_v)$ . In other words, the execution intervals of the observer task can only appear at time columns  $[0, \delta_v)$  and  $[\delta_v + bect_v, p_v)$ . Therefore, the execution intervals of the observer task will not be present at the true arrival column ( $\delta_v$ ) and also it would have been preempted.

### B.3 Proof for Theorem 4.1

From Observation 2, the time column offset of the observer task's execution repeats every  $LCM(p_o, p_v)$ . Therefore, the aforementioned condition (i.e., the scheduled execution of  $\tau_o$  appears in all possible time columns) can be described by the inequality  $\frac{LCM(p_o, p_v)}{p_o} \cdot e_o \geq p_v$ . Then, by using  $LCM(p_o, p_v) = \frac{p_o p_v}{GCD(p_o, p_v)}$ , we can derive a condition for  $e_o$  that guarantees that the observer task can detect the arrivals of the victim task to be  $e_o \geq GCD(p_o, p_v)$ .

### B.4 Proof for Theorem 4.3

From Theorem 4.1, if  $e_o \geq GCD(p_o, p_v)$  (i.e.,  $\mathbb{C}(\tau_o, \tau_v) \geq 1$ ), then the observer task's execution can appear in all time columns in the schedule ladder diagram which contain the true arrival column  $a_v$ . Thus the true arrival time column is enclosed in the observer task's execution. If  $e_o < GCD(p_o, p_v)$  (i.e.,  $0 \leq \mathbb{C}(\tau_o, \tau_v) < 1$ ), then the observer task's execution can only appear in some time columns in the schedule ladder diagram. The true arrival time column  $a_v$  may not be observable by the observer task's execution, thus the observer task may not be able to infer the correct information about  $\tau_v$ .

### B.5 Proof for Theorem 4.4

From Equation 2, the coverage of given  $\lambda$  can be computed by  $\frac{\lambda}{GCD(p_o, p_v)}$ . Theorem 4.1 indicates that  $\mathbb{C}(\tau_o, \tau_v) = 1$  is enough to ensure that the execution of the observer task can cover all  $p_v$  time columns once. Therefore, for Condition 1 where  $\mathbb{C}(\tau_o, \tau_v) \geq 1$ , the one-time coverage of all  $p_v$  time columns by  $\lambda$  is represented by  $\frac{\lambda}{GCD(p_o, p_v)} = 1$  which leads to the result  $\lambda = GCD(p_o, p_v)$ . For Condition 2 where  $\mathbb{C}(\tau_o, \tau_v) < 1$ , based on Theorem 4.3, the coverage by the execution of the observer task is not enough to cover all  $p_v$  time columns. In such a case,  $\lambda = e_o$  should be used to gain the most coverage, which is equal to  $\frac{e_o}{GCD(p_o, p_v)}$ .



### C AN EXAMPLE FOR THE SCHEDULEAK ALGORITHMS

Consider a system that has the real-time task set  $\Gamma = \{\tau_1, \tau_o, \tau_v, \tau_4\}$ . For the sake of simplicity, we assume that all tasks are periodic tasks in this example (though our analysis can work with periodic, sporadic and mixed systems as well). The task parameters are presented in the table below (on the left). Note that  $pri_i > pri_j$  means that  $\tau_i$  has a higher number than  $\tau_j$ . Thus, task  $\tau_1$  has the lowest priority while task  $\tau_4$  has the highest priority and  $\tau_v$  has higher priority than  $\tau_o$ . Let the maximum reconstruction duration  $\lambda$  be 1 and the start time of the attack be 0 (as a result,  $a_v$  equals  $\delta_v$  in this example). Assuming the attacker has executed the first step/algorithm for some duration, the table on the right hand side lists the reconstructed execution intervals of the observer task.

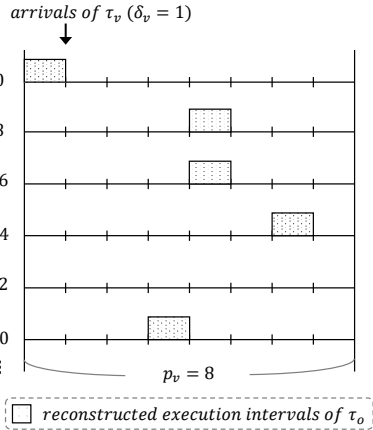
	$p_i$	$e_i$	$a_i$	$pri_i$
$\tau_1$	15	1	3	1
$\tau_o$	10	2	0	2
$\tau_v$	8	2	1	3
$\tau_4$	6	1	4	4

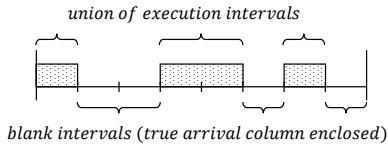
Reconstructed Execution Intervals
[0,1)
[12,13)
[20,21)
[30,31)
[43,44)

Note that since  $\tau_1$  has priority lower than the observer task  $\tau_o$ , it does not influence the execution of  $\tau_o$ . Then, we place the reconstructed execution intervals in a schedule ladder diagram of width equal to the victim task's period  $p_v$ . This operation is shown in Figure 13(a).

From the schedule ladder diagram in Figure 13(a), we perform a union of the execution intervals in each time column. The results are shown in Figure 13(b) – essentially a set of execution intervals and empties. The empty intervals (*i.e.*, ones without execution intervals) are candidate time columns that contain the true arrival column



(a) Placing the reconstructed execution intervals in the schedule ladder diagram.



(b) Calculating union of the reconstructed execution intervals.

Figure 13: Process of creating the schedule ladder diagram for the example in Appendix C.

we want to extract. These empty intervals are passed to the final step to infer the initial offset/arrival times of the victim task.

The obtained intervals correspond to the time columns [1, 3), [5, 6) and [7, 8). According to the algorithm, the largest interval, [1, 3), is selected. The beginning point of such a interval is then taken as the inference of the victim task's true arrival column, which becomes  $\delta_v = 1$ . In this example, the true arrival column is  $\delta_v = 1$ . Therefore, the algorithms correctly infer the true arrival column of the victim task and the initial offset can be derived accordingly.

To better understand the effectiveness of the schedule ladder diagram in profiling the victim task's behavior, we plot the original, complete, schedule of this example on the ladder diagram in Figure 14 so that readers get a better sense of it. This is not a part of the algorithms, but this gives us an insight into the correlation of the behaviors between the observer task and the victim. The diagram shows that time columns [1, 3) are always occupied by either the victim task or other higher priority tasks. Therefore, the execution intervals of the observer task will not land on these time columns where the true arrival column is enclosed. This fact is what the proposed algorithms is based on.

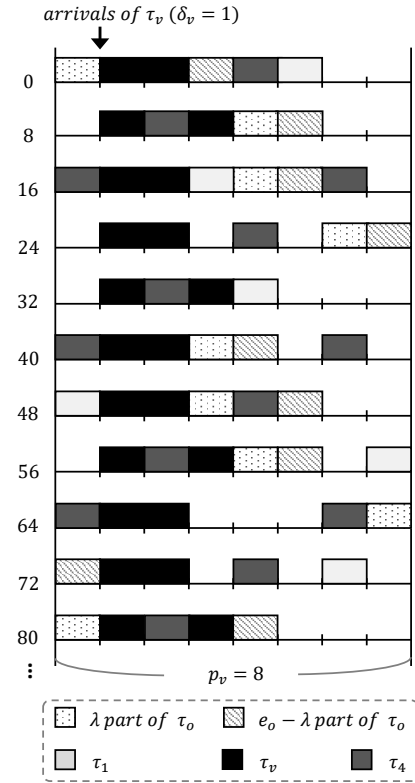


Figure 14: The schedule ladder diagram with placing the schedule in it. The schedule ladder diagram has a width of  $p_v$ . It shows the correlation between the observer task's execution and the victim task on the schedule ladder diagram. Note that this is not a part of the proposed algorithm.

## D TABLE FOR THE ATTACK DURATION EXPERIMENT

Table 2: Summary of the success rate and the inference precision ratio for the experiment shown in Figure 7.

DU*	Success Rate	Inference Precision Ratio				
		Mean	SD	Min	Median	Max
1	53.65%	0.8136	0.2938	0	1.0	1.0
2	86.69%	0.9527	0.1683	0	1.0	1.0
3	94.52%	0.9835	0.0987	0	1.0	1.0
4	96.68%	0.9912	0.0694	0	1.0	1.0
5	97.08%	0.9924	0.0641	0	1.0	1.0
6	97.37%	0.9935	0.0586	0	1.0	1.0
7	97.67%	0.9936	0.0596	0	1.0	1.0
8	97.70%	0.9940	0.0575	0.02	1.0	1.0
9	97.76%	0.9938	0.0595	0.01	1.0	1.0
10	97.59%	0.9933	0.0606	0	1.0	1.0

\*Duration is based on  $LCM(p_o, p_v)$ .